Tin Titanate – the hunt for a new ferroelectric perovskite

Tin Titanate – the hunt for a new ferroelectric perovskite

J. Gardner,[1] Atul Thakre,[2,3] Ashok Kumar,[2,3] J. F. Scott,[1,4]

1 School of Chemistry, University of St. Andrews, St. Andrews, KY16 9ST, United Kingdom
2 CSIR-National Physical Laboratory (CSIR-NPL), Dr. K. S. Krishnan Road, Delhi 110012, India
3 Academy of Scientific and Innovative Research (AcSIR), CSIR-NPL Campus, Dr. K. S. Krishnan Road, Delhi 110012, India
4 School of Physics and Astronomy, University of St. Andrews, St. Andrews, Fife KY16 9SS, United Kingdom

Email: ashok553@nplindia.org and jfs4@st-andrews.ac.uk

Abstract

We review all the published literature and show that there is no experimental evidence for homogeneous tin titanate $SnTiO_3$ in bulk or thin-film form. Instead a combination of unrelated artefacts are easily misinterpreted. The X-ray Bragg data are contaminated by double scattering from the Si substrate, giving a strong line at the 2-theta angle exactly where perovskite $SnTiO_3$ should appear. The strong dielectric divergence near 560K is irreversible and arises from oxygen site detrapping, accompanied by Warburg/Randles interfacial anomalies. The small (4 $\mu C/cm^2$) apparent ferroelectric hysteresis remains in samples shown to be pure $(Sn,Ti)O_2$ rutile/cassiterite, in which ferroelectricity is forbidden. Only very recent work reveals real bulk $SnTiO_3$, but it possesses an ilmenite-like structure with an elaborate array of stacking faults, not suitable for ferroelectric devices. Unpublished TEM data reveal an inhomogeneous SnO layered structured thin films, related to shell-core structures. The harsh conclusion is that there is a combination of unrelated artefacts masquerading as ferroelectricity in powders and ALD films; and only a trace of a second phase in PLD film data suggests any perovskite content at all. The fact that X-ray, dielectric, and hysteresis data all lead to the wrong conclusion is instructive and reminds us of earlier work on copper calcium titanate (a well-known boundary-layer capacitor).

Key words: Ferroelectric, lead-free, room-temperature, tin titanate.

Ferroelectrics are technologically and commercially important materials used in a wide range of applications including as capacitors, memories and for applications utilising their piezoelectric and pyroelectric properties. A large proportion of commercial devices use the ubiquitous ferroelectric material lead zirconate titanate (PZT, $PbTi_{1-x}Zr_xO_3$), due to high T_C, large polarisation, etc. Lead titanate and PZT with c.a. > 50 % Ti^{4+} adopts a highly tetragonal ABO_3 perovskite structure below T_C due to the Pb^{2+} lone pair, however, the deleterious effects of lead on the environment and human health have led to the search for lead-free ferroelectrics.

Tin is within the same group of the periodic table as lead, and like Pb^{2+}, Sn^{2+} possesses an electron lone pair. However, while $PbTiO_3$ and PZT are well known materials, this is not the case with perovskite $SnTiO_3$. Conversely, perovskites with tin in a 4+ oxidation state occupying the B site, *e.g*. $BaSnO_3$, have been reported since the mid-20th century. [1]

Interest in perovskite $SnTiO_3$ was renewed due to recent theoretical/computational studies [2-13], many of which predicted that this material would be a stable, lead-free, room-temperature ferroelectric with high switched polarisation (ca. 100 $\mu C/cm^2$), [5,8,12] capable of replacing PZT for many device applications. There are of course other lead-free room temperature ferroelectrics that might replace PZT for many commercial applications. However, $SnTiO_3$ is unusually attractive because it is comprised of cheap and relatively safe ingredients in what was expected to be a robust structure, and in particular had a very large theoretical polarisation. In that sense it was, and remains, of great commercial interest, which has therefore led to renewed efforts to synthesize perovskite structured $SnTiO_3$ in both bulk and film forms [14-20].

Substitution of small amounts of tin into existing perovskite structures is possible although the resulting site occupation appears to differ – e.g. in $(Ba,Ca)TiO_3$, Sn^{2+} primarily occupies the A-site [21], yet in $SrTiO_3$ compounds occupation of both A- and B-sites is reported [22-25] . This difference may simply be related to the control of the tin oxidation state with the larger Sn^{2+} preferentially occupying the A-site and smaller Sn^{4+} the B-site. Moreover, it is not impossible to form other homogeneous stable Sn^{2+} oxides including tungstates and titanates, as shown by the work on Sn_2TiO_4 [26] , $SnNb_2O_6$ [27], $SnTa_2O_6$ [28] and $SnWO_4$. [29]

Due to the predicated attributes of perovskite structured $SnTiO_3$ and its potential as a lead free device material, numerous synthetic methodologies have been employed over a number of years with limited success. Traditional solid state synthesis methods, employing high

temperature reactions, have been unsuccessful due to the disproportionation of SnO and oxidation of Sn^{2+} at elevated temperatures. [30] Reports of such solid state reactions are largely absent from the published literature due to this lack of success. The notable exception is a Bachelor's thesis which reports a number of synthetic routes, including solid state and sol-gel reactions, performed under various atmospheres and over a wide range of temperatures.[18] No perovskite structured material was produced, although a rutile structured $SnTiO_4$ [$(Sn,Ti)O_2$] was formed using aqueous methods and low temperature reactions.

Most recent work has focused primarily on using soft chemistry routes, such as sol-gel or co-precipitation, and thin-film techniques. In this review we examine the current literature reporting experimental studies of $SnTiO_3$.

Co-precipitation from chlorides

Conventional solid state methods employing high sintering temperatures typically lead to oxidation/disproportionation of Sn^{4+} precursor reagents. Attempts to prevent the oxidation of the Sn^{2+} have included "soft" chemistry preparation routes which typically permit lower sintering temperatures and superior admixing compared with traditional solid state methods. Two papers report attempts to produce samples of $SnTiO_3$ via a co-precipitation method using $SnCl_2$ and $TiCl_4$ as starting materials [14, 15].

The first, [14] refers to "perovskite type tin titanate ($SnTiO_3$)" in the introduction while discussing its proposed properties, however, while the author discusses "tin titanate" and refers to "$SnTiO_3$ powders" the structural data reported are sparse. The paper states that "the formation of tin titanate is evidenced by the characteristic peak of tin titanate in the XRD spectrum" and lists the positions of three peaks from a powder X-ray diffraction (PXRD) pattern measured from powders calcined at 850 °C. However, no PXRD database pattern or crystallographic model is referenced and all other structural/crystallographic information is absent – symmetry (space group and point group), lattice parameters, atom positions, etc. are not reported.

The positions of the three peaks (31.8°, 33.5° and 39.8° 2θ) are similar to those of a simulated perovskite tin titanate pattern published in Ref. [19], based on calculations from previous theoretical studies [5, 12]. This would suggest a large tetragonal strain (cell of $a \approx b \approx 3.80$ Å and $c \approx 4.09$ Å from [19]. However, other tin-titanium containing oxides possess PXRD peaks

close to these 2θ positions listed (e.g., simulated PXRD patterns from crystallographic models from the Inorganic Crystal Structure Database (ICSD) - collection codes 161282, 410690, 30664 [31-33]). As bulk perovskite structured $SnTiO_3$ would be a novel and commercially important material, it is difficult to conclude that ref [14] successfully synthesized the material, due to the lack of structural data presented. Additionally, no dielectric or ferroelectric properties were studied.

A subsequent paper by a different group used a similar co-precipitation method [15] and unambiguously describe the resulting compound as perovskite. Greater details of structural studies are provided, however, the paper is somewhat contradictory; they describe the formation of a new phase and list PXRD peak positions (21.62, 29.01, 33.4, 34.8, 37.8, 49.09, 50.96 and 59.8° = 2θ) cited from an abstract of a master's thesis from which the peak positions were obtained. [34] The thesis abstract, (which appears to be available only via a dissertation publishing site) states that the PXRD peaks of their material, obtained from a different synthetic route, was difficult to match to a Powder Diffraction File card (a reference pattern from database). The authors of Ref [15] then cite Ref [14] when describing their PXRD data as having "characteristic peroveskite (*sic*) structural values", however, other than the peak at 33.4° the other two values from Ref. [14] do not match those listed above. Furthermore, there are several issues with the accompanying PXRD pattern: there is a greater number of peaks than those listed in the text, there appears to be two different sets of peaks with dissimilar peak broadness overlying each other (it is not stated if one set is a reference pattern and information on the symbols over certain peaks is likewise omitted), and the figure image is blurred to an extent that the axis scales are illegible. Therefore, based upon this early work by itself, one cannot definitively conclude that perovskite $SnTiO_3$ was synthesized.

$SnTiO_3$ PLD films

The deposition of materials in the form of thin films has various technological advantages and has additionally enabled materials to be formed which are unstable in the bulk form. As such, much recent work on tin titanate has concentrated on the fabrication of thin films using a number of deposition techniques.

Such films have been deposited using pulsed laser deposition (PLD) on a number of different perovskite structured substrates, with a unit cell close to that of the desired $SnTiO_3$ phase [16]. One of the disadvantages of film deposition is the usually limited amount of information

obtained using standard laboratory diffraction (i.e. x-ray diffraction, XRD) techniques due to the presence of only a small amount of material which is often orientated such that only a small number of crystallographic planes satisfy diffraction conditions. Typically only a small number of sometimes weak peaks may be observed. As such, only one Bragg peak is observed in their diffraction data, Fig. 1, which in isolation is somewhat inconclusive. However, their electron diffraction data, Figure 2, shows a triclinic cell consistent with an ilmenite $SnTiO_3$ structure with $\alpha = 90°$, $\beta = 90°$, $\gamma = 120°$, and lattice dimensions of $a = 5.04$ Å, $b = 5.19$ Å, $c = 14.56$ Å. In discussing why the ilmenite structure is formed the authors of Ref [16] note that, while a number of theoretical studies predict a perovskite $SnTiO_3$ structure, Ref [35] calculates that the ilmenite structure is more stable in a reducing atmosphere.

The PLD films produced in Ref. [16] do not exhibit any indication of ferroelectricity under measured conditions, however, in reciprocal XRD space maps additional weak lines were detected which do not originate from the substrate or ilmenite phase. The authors of [16] propose that this minor may originate from very small quantities of perovskite, with inferred unit cell of $a = b = 3.76$ Å and $c = 4.18$ Å, similar to those predicted theoretically for perovskite $SnTiO_3$. [12, 16] We note that Ref. [9] conclude that $SnTiO_3$ is stable in P4mm structure only for $a,b < 3.87$ Å and distorts to monoclinic *Cm* (*C*1*m*1) for larger lattice constants.

Using a tetragonal perovskite structural model, we have simulated an XRD pattern, Figure 3, of this phase to determine the 2θ positions of the Bragg peaks as they would appear with Cu $K\alpha_1$ radiation. The perovskite structural model used was modified from a $PbTiO_3$ structure from the Inorganic Crystal Structure Database (collection code 61168, [36]) with space group *P*4*mm* as this symmetry has previously been used in computational/theoretical studies of perovskite $SnTiO_3$. [2, 37] Pb^{2+} was replaced by Sn^{2+} at the A-site and the lattice parameters were altered to those reported from the PLD film [16] – no other changes were made e.g. to atom positions. The three peak positions reported in the chloride synthesis work [14] discussed above, are close to those in the simulated pattern. Oxides of tin and titanium and metallic tin also have peaks close to those three 2θ values and the powder in [14] had been heated to 850 °C at which Sn^{2+} compounds usually decompose/disproportionate [30] Therefore, while this is not enough to conclude that perovskite $SnTiO_3$ was actually made in Ref [14], it does demonstrate that the values are consistent with the minor perovskite phase present in the PLD films.

$YMnO_3/SnTiO_{3+x}$ heterostructure PLD films

Later work by another group attempted to stabilise tin titanate by growing PLD films with alternating layers of $YMnO_3$, to produce $YMnO_3/SnTiO_{3+x}$ composites with varying numbers of layers [19]. These films were deposited on (100), (111) and (110) Nb:$SrTiO_3$ (Nb:STO) substrates with 2, 4 or 8 layers. XRD peaks from these films, Figure 4, were attributed in the paper to: ilmenite [two layer film deposited on (100) Nb:STO], a mix of perovskite and ilmenite [4 layer films on (100) and (110)], perovskite and an unidentified phase [4 layers on (111)] and perovskite [8 layers on (100)]. As seen in Figure 4, with the exception of a peak at approximately 33° two theta, the presence and appearance of the other peaks assigned to a perovskite structure changes with layer number and substrate orientation and while this may be due to the orientation of the film (or strain etc.), the authors do not discuss this or any possible origin. They do note the need for further structural characterisation using TEM and state their intension to carry this out, however, no further papers appear to have been published to date.

P-E data, Fig. 2 in Ref [19], on the 2 layer film (ilmenite XRD) shows a very small measured polarisation of < 0.05 $\mu C/cm^2$ which would be consistent with the non-polar $FeTiO_3$ ilmenite structure they assign and with the linear P-E response (*i.e.* not ferroelectric) obtained from the principally ilmenite PLD film discussed earlier [16]. For films with four or more layers they measure a larger polarisation but somewhat lossy P-E loops and state that "contributions to the hysteresis loop from movable charges was significant" in certain films. Charge injection is one of a number of artefacts found in bulk and thin films which may obscure the true properties of a material. [38-41] PFM data also indicates possible switching, however, as seen later in recent PFM work on ALD films, possible charging effects may be misleading. Without PUND or TEM measurements and additional PFM experiments, some ambiguity remains. Additionally, the contribution from the intrinsic magnetic and ferroelectric properties of the $YMnO_3$ layers or from interfacial effects is unclear making it difficult to establish the properties of the $SnTiO_{3+x}$ components of the film structure.

ALD films

Atomic layer deposition (ALD) was used by the authors of ref [42] to obtain films with the aim of producing perovskite structured $SnTiO_3$. Using titanium and tin precursors, TDEAT and $Sn(acac)_2$, films of tin titanate ($SnTiO_x$) were deposited on Si(100) substrates. This synthesis method typically uses lower reaction temperatures and allows better control of oxidation states

and composition through the variation of the annealing conditions of the deposited film [43-46]. Deposited films were annealed under different atmospheres (O_2, N_2 and H_2) at 350 and 650 °C for 5 mins. Using grazing incident angle X-ray diffraction (GIXRD) they found anatase appeared to be the major phase present on both as-deposited and annealed films. This was based on assigning two broad peaks at c.a. 55 degrees 2θ to the 105 and 211 reflections from the anatase structure. However, piezoelectric switching hysteresis loops were demonstrated on films annealed at 350 °C under O_2, [42,43] which led to additional studies on the film [17], including polarisation-electric field (P-E) and dielectric measurements as well as further PXRD data.

Polarisation-electric field (P-E) measurements yielded hysteresis loops with a remanent polarisation of 3μC/cm^2 at room temperature and further PUND data was used to determine the existence of switched polarisation in the film [17]. The latter measurement uses a different pulse sequence from typical dynamic P-E measurements, consisting of two successive electrical pulses of the same polarity. Assuming the ferroelectric material is switched during the initial pulse, the second pulse should have no contribution originating from the switching of ferroelectric domains and therefore reveal contributions from extrinsic sources such as leakage current. [47] This is, however, not always the case due to e.g. relaxation. Dielectric data on this film showed a frequency dependent peak with $T_m \approx 450 - 600$ K, as shown in Fig3(a) of Ref [17].

Additional peaks were observed in XRD, although the data are somewhat complicated by the presence of a nominally forbidden Si(200) peak overlying a peak at 33° 2θ which was attributed to the film. This substrate peak is basis-forbidden but may be present in diffraction patterns due to multiple (double) diffraction (a process also known as Umweganregung) [48, 49]. Bragg peaks in XRD patterns originate from the diffraction of incident X-rays from lattice planes of a crystalline material. In the case where nominally forbidden Bragg peaks are observed due to multiple diffraction, the incident X-rays have previously diffracted from a lattice plane rather than originating directly from the X-ray source. The forbidden peak may have variable intensity and exhibit shoulders and sub-peaks at approximately 33 ±2.5° = 2θ, as shown in Figure 1 of Ref [48]. PXRD patterns of the substrate lack any such shoulder, Figure 5.

It has previously been demonstrated that when measured on PXRD diffractometers operating in Bragg-Brentano geometry, the intensity of this forbidden peak varies with Φ, the angle normal to the plane surface of the sample [49]. On such diffractometers it is common to spin

the sample within this axis to improve the quality of the data collected, which leads to an averaging of the diffraction from all Φ angles. New data, Figure 5, on one of the ALD films were collected during which the sample was not spun, and as can be seen both the sharp forbidden Si peak and that assigned to the perovskite film, are absent. A peak at high angle (c.a. 117 ° = 2θ) also coincides with a possible Si peak, leaving only the peak around 55° = 2θ which consistently occurs in conventional XRD and GIXRD; therefore the structure of the film as determined by X-ray diffraction is somewhat ambiguous. Hence, despite significant improvements over the earlier data from bulk powder samples, the XRD results are by themselves inconclusive.

AFM/PFM has thus far failed to reveal any ferroelectric domains in these samples or in the ALD films studied previously. There are several possible reasons: (a) Any domains are expected to be very small (<30 nm), since the grains are very small, where previously measured; (b) the samples almost certainly are heterogeneous, and the outermost surface layer is ca. 15 nm thick, according to TEM; (c) the surfaces do not appear to be extremely clean, and attempts to clean them may destroy the films. Strong surface charging of half-surfaces occurs, Figure 6; however, as no domains are visible, this may just be surface charging of the whole sample.

To ascertain if charge writing is being observed electrical force microscopy was performed. Two surface areas of the ALD films (indicated by boxes in Figure 6) with opposite polarities were written and then electrical force microscopy preformed to probe surface charging. EFM signal is usually indicative of charge being injected into surfaces for a myriad of reasons. As seen in Fig. 6, the signature of charge writing in the written boxes is evident. This signature stays for a few scans meaning it could explain the signal decay seen in piezoresponse images, Fig. 7. This does not rule out ferroelectricity completely but does explain the lack of retention of the written states.

Sol-gel

In an attempt to reconcile some of the results discussed above, a sol-gel method was used to produce tin titanate ($SnTiO_x$) nanoparticles. The two precursors were initially dissolved in solvent; tin acetate in methanol and titanium (IV) isopropoxide in a 1:1 ratio of glacial acetic acid and 2-methoxy ethanol. These were combined and stirred for half an hour and the resulting

solution heated at 250 ºC on a hot-plate for 24 hrs. The obtained nanoparticles were calcined at 550 ºC for 4 hrs. Circular pellets, with diameter and thickness of 10 mm and 0.650 mm respectively, were pressed and sintered at 550 ºC for 4 hrs. In order to carry out the electrical measurements electrodes of an In-Ga alloy were applied to the circular faces of the pellet.

PXRD data are shown in Figure 8. Bragg peaks exhibit extensive broadening, likely size-broadening due to the small size of the crystallites (determined to be c.a. 8-10 nm from TEM). Peak positions are consistent with a rutile structure and Rietveld refinement using a rutile structural model (Inorganic Crystal Structure Database, ICSD, collection code – 161282) accounts for all peaks and gives a reasonably good fit (goodness of fit parameters $\chi^2 = 1.4$, $R_{wp} = 0.129$, R(F2) = 0.12). The crystallographic model used originated from ref [50] and is a tetragonal rutile structure, space group $P4_2/mnm$, with composition $Sn_{0.39}Ti_{0.61}O_2$. Unit cell dimensions of $a = b = 4.67$ Å $c = 3.08$ Å were obtained from refinement of the PXRD data. These values are somewhat intermediate of those of rutile structured TiO_2 and SnO_2 (cassiterite), [51] which is unsurprising as Sn^{4+} is larger than Ti^{4+} [52].

It should be noted that PXRD is a bulk technique which obtains the spatially averaged structure and that Ti-Sn segregation can occur [53]. SEM and TEM data, Figures 9 and 10 show nano-crystallites with homogenous morphology. SEM/EDAX gives a 1.1:1 Sn:Ti ratio. This ratio is consistent with both rutile and perovskite structures. HRTEM data also gives 110 planes with d-spacing of 0.33 nm.

Raman spectroscopy was performed on the surface of pellets. The odd-parity zone-centre vibrations in the cubic phase have been calculated as [ ]: TO(1), soft (imaginary frequency); LO(1), 80 cm-1; TO(2), 126 cm-1; LO(2), 375 cm-1; TO(3), 505, cm-1; and LO(3), 689 cm-1. A few experimental values have been reported [7] for wave numbers above 400 cm-1, but they are not in close agreement with predictions, with phonons at 455 cm-1, 619 cm-1, and slightly less than 800 cm-1. As expected, these are close to those in rutile TiO_2 or rutile-structure cassiterite SnO_2 (the latter at 474, 632, and 774 cm-1). [,]

Raman data were obtained for the ambient temperature phase in the present work (Table 1 and Fig. 11) but symmetries are uncertain. Even if there were comparable amounts of rutile-structure and perovskite, the Raman spectra of the latter would be much weaker because in the cubic perovskite phase first-order Raman scattering is forbidden (all ions at inversion centres); so the spectra might be dominated by cassiterite/rutile.

Table 1. Phonon frequencies in tin titanate

Calculated (present work)	**Symmetry phase**	**Experiment**	**LO Cubic SnO_2**	**Rutile TiO_2**	**Cassiterite cm^{-1}**
90	E(TO)	100			
134	E(LO)	140	80	143 B_{1g}	123 B_{1g}
218	E(TO)	---			
230	E(LO)	---			
232	A1(TO)	---			
243	A1(LO)	248			
319	E(TO)	---			
399	A1(TO)	---			
448	E(LO)	442	375	443 E_g	474 E_g
462	A1(LO)	---			
530	E(TO)	---			
633	E(LO)	628		610 A_{1g}	632 A_{1g}
704	A1(TO)	---			
820	A1(LO)	798	689	844 B_{2g}	774 B_{2g}

Dielectric measurements as a function of temperature are presented in Fig. 12. Frequency-dependent features in both the relative permittivity and normalised loss, tan δ, occur at similar temperatures to that of the dielectric peak observed in the ALD film [17]. However, these features are only observed on heating – they are largely absent on cooling, Fig. 12(c) and (d) and during further heating and cooling cycles. The samples were sintered at 550 °C for 4 hours and so the observed behaviour is unlikely to originate from a transformation to a new phase.

Unfortunately, it is well established that non-ferroelectric materials deposited onto semiconducting or metal blocking electrodes can sometimes produce large dielectric peaks in the 200-500 C temperature regime which typically exhibit a frequency dependence [54]. Replacement of the Schottky electrodes Ag or Au with more ohmic contacts such as In-Ga also provides discrimination between intrinsic dielectric peaks and electrode contributions.

Non-ferroelectric $(Sn,Ti)O_2$ compounds, which have been studied for use as a potential device material for gas sensors and varistors, also display complex conductivity and dielectric properties.[55] These issues include: the existence of non-ohmic grain boundaries in transition metal doped SnO_2,[56] immiscibility of tin/titanium, [55], reported different conduction processes - band conduction in SnO_2 and hopping in TiO_2 [57] and differences in conduction with thermal cycling. [58]

Impedance data is also similarly complex - the impedance complex plane (Cole-Cole) plot measured at 475 K shown in Figure 13 gives what appears to be a semi-circle and a low frequency tail, indicative of a Warburg element [59, 60]. This resembles the response obtained from a Randles circuit, an equivalent circuit which is often used to model processes at interfaces [59, 60]. Not only is it extremely linear over a long range, but it makes the required angle of 45 degrees (gradient of slope is 1.00, Figure 14). Equivalent circuit models should not be derived from single data sets as it is often the case that other electroactive regions within the sample simply do not contribute to the data at that specific temperature (*i.e*. their time constant is outside the spectroscopic measuring window). With increasing temperature the low frequency tail becomes non-linear before forming an additional semi-circle. The higher frequency section of this new feature is still somewhat linear initially (Figure 14) – it is therefore difficult to determine if the 'tail' represents true diffusion, as Warburg elements are normally interpreted, or merely the high frequency response of the other feature moving into the measured frequency range. If it is the former, such linearity has previously been attributed to a change from semi-infinite to finite length diffusion,[59] with the linear region being described as the "transition region".[60]

There is also a large and as yet unexplained change in sample resistance of x100. We attribute all these phenomena in dielectric response near T=500K, including the "Warburg" element as due to abrupt emptying of oxygen traps. Artefacts from e.g. the electrode-interface effects and oxygen vacancy de-trapping etc. are common [54], and the observed features in dielectric and impedance data are likely to be extrinsic in origin. The inference of oxygen site depinning is not just an unsupported hypothesis. The reversible surface charging (Fig.6 and 7) reported in the new AFM study of the ALD films (bright metallic with +10 V applied; dark with -10V applied) is compatible with that, as is the lack of domain walls in the AFM images.

Polarisation-electric field (P-E) measurements on the pellets are shown in Figure 15 (a). A linear (albeit slightly leaky) dielectric response is obtained at 100 Hz; with decreasing frequency the loop opens up, however, this is unlikely to be due to ferroelectric switching. These hysteresis loops are reproducible but cannot be intrinsic, since they do not evidence a Curie temperature above which they disappear and are present in specimens that are shown to be pure rutile/cassiterite. They may arise from charge trapped at the electrode-dielectric interface and as discussed previously we suspect they are oxygen traps.

PUND data (measurement described previously for ALD films and more generally in Ref [47]) of these samples indicate little or no actual switching of polarisation, Fig 15(b). The value of polarisation for successive pairs of pulses (P and U; N and D) are very similar which suggests that the primary switching pulses (P and N) do not contain a contribution from the switching of domains – i.e. that the response is purely extrinsic.

Bulk $SnTiO_3$ using soft chemistry

Most recently a bulk form of $SnTiO_3$ has been successfully produced using a soft chemistry method. [20] To avoid oxidation/disproportionation of Sn^{2+} the authors of Ref [20] used a multi-step metathesis synthesis by first forming a layered $K_2Ti_2O_5$ compound. This was heated with $SnCl_2.2H_2O$ at 300 °C under vacuum for 24 hours, after which the KCl salt by-product was removed with washing, leaving $SnTiO_3$. However, this bulk $SnTiO_3$ powder does not contain perovskite, instead forming an ilmenite-like structure [20] which could not be indexed directly to the conventional ilmenite structure as identified in the previous PLD films.[16] This was due to the highly layered nature of the structure with ilmenite-like slabs separated by van der Waals gaps from the lone pairs of Sn^{2+} and as a result forming multiple stacking orders and twin domains [20]. A combination of a number of polytypes, each modelling different stacking sequences, was required to account for the observed structural data, with electron energy loss spectroscopy and nuclear magnetic resonance data supporting the resulting local structure/symmetry.

Despite the structural complexity introduced by the different stacking sequences, the bulk $SnTiO_3$ obtained by this group shares similarities most with the PLD films produced in Ref [16] – i.e. the major product is ilmenite or an ilmenite-like structure rather than perovskite. The non-layered nature observed in the PLD films may simply be a consequence of the synthesis method. Diehl et al. calculated that the different stacking sequences were

comparable in energy in the bulk form and that, using electron localisation function and density functional theory, the lone pairs of the Sn^{2+} directed the structure. [20] In the PLD films strain, low dimensionality, synthesis temperatures etc. seems to favour the simpler ilmenite structure. Another possible explanation is the role of the layered $K_2Ti_2O_5$ starting material.

Conclusions

Perovskite ferroelectric tin titanate has not yet been made in thin films or bulk as single-phase material. It clearly does exist, for example in a minor phase prepared via PLD, and possibly as a single-phase powder via titanium chloride processing. Despite its toxicity, this process should be examined further in laboratories with proper safety facilities.

The electrical data are largely dominated near T=500K by abrupt emptying of oxygen traps, not a ferroelectric phase transition. AFM shows that these surfaces can be emptied or filled via +10V and –10V but that domains do not form.

The PUND switching data are in themselves not unambiguous evidence of ferroelectricity.

Several studies suggest highly inhomogeneous products, with nano-phase separation. This may account for differences in published XRD data.

As a Key Issues Review, this report is not intended to be the definitive story, but merely a guide to help new researchers through the literature, which is not all self-consistent.

The synthesis of bulk perovskite $SnTiO_3$ presents many problems including the thermal stability of the SnO and propensity of Sn^{2+} to oxidation. Additionally, Sn^{4+} in the B-site of perovskites and related structures appears to inhibit ferroelectricity. [61] Preparation routes which preserve (or generate) Sn^{2+} are needed to both produce the perovskite structure and for optimal ferroelectric properties.

Does the extreme difficulty in preparing these tin compounds in the Sn^{2+} valence state make further work unwise? If not, what approaches might be tried next? At present the results show that the products obtained are usually ilmenite or cassiterite/rutile (without mixed phases), depending upon processing parameters. However, some nano-layer results have been found at U. Conn., for which we do not have permission to reproduce. So the production of inhomogeneous layered or core-shell samples might be possible.

We suggest future studies into the soft chemistry synthesis method which produced bulk ilmenite $SnTiO_3$ in Ref [20], including investigating the possibilities of changing reaction conditions or the potassium intermediate structure to influence the stacking arrangements of ilmenite or favour the formation of perovskite $SnTiO_3$. Other synthesis methods may also be worth considering including high pressure and newer cold sintering methods. Work on the densification of tin monoxide, SnO, has recently been reported using cold sintering, [62] and the technique has previously been used to produce PZT and $LiFePO_4$. [63] The low temperatures employed may allow the preservation of the Sn^{2+} state, allowing stoichiometric $SnTiO_3$ to be formed, possibly with the perovskite structure.

Generally speaking, however, this does not look like a thesis project at a typical university now, but instead might require a larger, better-funded industry effort to stabilize Sn^{2+} valences in the presence of oxygen, perhaps involving two-step processes. Thus far, PLD, ALD, and conventional solid state reactions have been emphasized, but more sophisticated deposition techniques might be tried. ALD has the advantage of lower processing temperatures. It is worth keeping in mind that $SrTiO_3$:Si has been successfully prepared in the past via MBE, most recently at modest temperatures [64-67] and earlier work succeeded in producing stable films via an intermediate atomic layer. [68]

Acknowledgements:

The synthesized materials at CSIR-NPL and related data may be requested to email: ashok553@nplindia.org. Amit Kumar for new PFM work on ALD films. Finlay Morrison. This work was supported in St Andrews by the Engineering and Physical Sciences Research Council (EPSRC) Grant No. EP/P024637/1

References

1. H.D. Megaw 1946 *Proc. Phys. Soc*. **58** 133

2. M. F. M. Taib , M. K. Yaakob , O. H. Hassan and M. Z. A. Yahya 2013 *Integ. Ferroelec*. **142**, 119

3. M. F.M. Taib, M. K. Yaakob, O. H. Hassan, A. Chandra, A. K. Arof, M. Z. A.Yahya 2013 *Ceram. Internat.* **39**, S297-S300

4. H. Ye, R. Zhang , D. Wang, Y. Cui, J. Wei, C. Wang, Z. Xu, S. Qu, and X. Wei 2013 *Int. J. Mod. Phys. B*, **27**, 0350144

5. Y. Uratani, T. Shishidou, T. Oguchi 2008 *Jpn. J. Appl. Phys*. **47**, 7735.

6. N. H. Hussin, M. F. M. Taib, N. A. Johari, F. W. Badrudin, O. H. Hassan, M. Z. A. Yahya 2014 *Mater. Eng. Adv. Technol*. **510**, 57

7. S. F. Matar, I. Baraille, M. A. Subramaniam 2009 *Chem. Phys*. **355**, 43.

8. W. D. Parker, J. M. Rondinelli, S. M. Nakhmanson 2011 *Phys. Rev. B*, **84**, 245136.

9. K. C. Pitike, W. D. Parker, L. Louis, and S. M. Nakhmanson 2015 *Phys. Rev. B*, **91**, 035112

10. C. Ma, X. He, K-J. Jin K-J 2017 *Phys. Rev. B*, **96**, 035140.

11. M. F. M. Taib, K. H. K. Arifin, M. K.Yaakob, A. Chandra, A. K. Arof, M. Z. A.Yahya, [A. Öchsner, L. da Silva, H. Altenbach (eds) *Materials with Complex Behaviour II, Advanced Structured Materials*, vol **16**. (Springer, Berlin 2012)].

12. Y. Konishi, M. Ohsawa, Y. Yonezawa, Y. Tanimura, T. Chikyow, T. Wakisaka, H. Koinuma, A. Miyamoto, M. Kubo and K. Sasata, 2002 *MRS Proceedings*, **748**, U3.13. doi:10.1557/PROC-748-U3.13

13. S. Suzuki, A. Honda, K. Suzuki, S. Higai, A. Ando, K. Niwa, and M. Hasegawa, 2013 *Jpn. J. Appl. Phys*. **52** 09KC04

14. K.S. Beenakumari 2013 *Int. J. Mater. Sci. Innovations* **1**, 174.

15. P. Sirajudheen and K.M. Muhammed-Ismayil 2015 *Chem. Sci. J*, **6**, 1000111

16. T. Fix, S. L. Sahonta, V. Garcia, J. L. M. Driscoll, M. G. Blamire 2011 *Cryst. Growth Des*. **11**, 1422

17. R. Agarwal, Y. S. Sharma, K. Chang, et al. 2018 *Phys. Rev. B* **97**, 054109.

18. T. Gubb 2013, Preparation routes for tin titanate perovskite, Bachelor thesis, Alfred University, viewed 3 March 2019, DOI: 10.13140/RG.2.1.4744.9207

19. H. Zhao, H. Kimura, Z. Cheng, X. Wang, Q. Yao, et al 2011 *Scrip. Materialia* **65**, 618

20. L. Diehl, S. Bette, F. Pielnhofer, S. Betzler, I. Moudrakovski, G. A. Ozin, R. Dinnebier, and B.V. Lotsch 2018 *Chem. Mater*. **30**, 8932

21. S. Suzuki, T. Takeda, A. Ando and H. Takagi 2010 *Appl. Phys. Lett*. **96**, 132903

22. S. Suzuki, T. Takeda, A. Ando, T. Oyama, N. Wada, H. Niimi and H. Takagi 2010 *Jpn. J. Appl. Phys.* **49**, 09MC04

23. S. Suzuki, N. Iwaji, A. Honda, S. Higai, N. Wada, A. Ando, and H. Takagi 2012 *Jpn. J. Appl. Phys*. **51**, 09LC08

24. S. Suzuki, A. Honda, N. Iwaji, S. Higai, A. Ando, H. Takagi, H. Kasatani, and K. Deguchi 2012, *Phys. Rev. B* **86**, 060102(R).

25. T. Wang, K. C. Pitike, Y. Yuan, S.M. Nakhmanson, V. Gopalan, and B. Jalan 2016, *APL Materials* **4**, 126111

26. N. Kumada, Y. Yonesaki, T. Takei, N. Kinomura, and S. Wada 2009 *Mater. Res. Bull.* **44**, 1298

27. T. S. Ercit and P. Cerny 1988 *Can. Mineral*. **26**, 899.

28. H. Mizoguchi, A.W.Sleight and M.A.Subramanian 2009 *Mater. Res. Bull*. **44**, 1022

29. W. Jeitschko and A. W. Sleight 1974 *Acta Crystallogr., Sect. B: Struct. Crystallogr. Cryst. Chem*. **B30**, 2088

30. H. Giefersa, F. Porschb, G. Wortmann 2005 *Solid State Ionics* **176**, 199

31. X. Yahong et al, 2008, *Chem. Mater*. **20**, 4931

32. B.A. Wechsler, and C.T. Prewitt, 1984, *American Mineralogist*, **69**, 176

33. H. Hillebrecht, and M. Ade 1999 *Z. anorg. allg. Chem*. **625**, 572

34. H.X. Qing and Z. P. Wen, 2013 A Challenge to Prepare Perovskite Structure $SnTiO_3$, TB34, 2-6 https://www.dissertationtopic.net/doc/1702829

35. G. Hautier, C.C Fischer, A. Jain, T. Mueller, G. Ceder 2010 *Chem. Mater*. **22**, 3762

36. R.J. Nelmes and W.F. Kuhs 1985 *Solid State Comm*. **54**, 721

37. M. F. M. Taib , M. K. Yaakob , F. W. Badrudin , T. I. T. Kudin , O. H. Hassan & M. Z. A. Yahya 2014 *Ferroelectrics*, **459**, 134.

38. L. Pintilie and M. Alexe 2005 *Appl. Phys. Lett* **87**, 112903.

39. R.K. Vasudevan, N. Balke, P. Maksymovych, S. Jesse, and S.V. Kalinin 2017 *Appl Phys Rev* **4**, 021302.

40. J.F. Scott and J. Gardner 2018 *Materials Today* **21**, 553.

41. J.F. Scott 2008 *J. Phys.: Condens. Matter*, **20**, 021001.

42. S. Chang, K. Selvaraj, Y.-Y. Choi, and S. Hong 2016 *J. Vac. Sci. Tech*. A **34**, 01A119

43. "Atomic Layer Deposition of Tin Titanate - Achieving Ferroelectricity And Beyond," Siliang Chang, PhD thesis, University of Illinois at Chicago, 2018

44. S. K. Selvaraj, A. Feinerman and C.G. Takoudis, J. Vac. Sci. Tech. A 2014, 32, 01A112

45. S. Chang and C.G. Takoudis, J. Vac. Sci. Tech. A 2018, 36, 01A121

46. S. Chang, S. Vijayan, M. Aindow, G. Jursich and C.G. Takoudis, J. Vac. Sci. Tech. A 2018, 36, 0315

47 K. Dimmler, M. Parris, D. Butler, S. Eaton, B. Pouligny, J.F. Scott and Y. Ishibashi, J. Appl. Phys. 1987, 61, 5467

48 P. Zaumseil, J. Appl. Cryst. (2015). 48, 528–532

49 B-H. Hwang J. Phys. D: Appl. Phys. 34 (2001) 2469–2474

50 Y. Xie, S. Yin, H. Yamane, T. Hashimoto, H. Machida, and T. Sato, Chem. Mater., 2008, 20, 4931

51. W.H. Baur, A.A. Khan, , Acta Cryst. Sect. B: Structural Crystallography and Crystal Chemistry, 1971, 27, 2133

52 R.D. Shannon, Acta Cryst. 1976, A32, 751

53 F. de la Pena, M.-H.Berger, J.-F.Hochepied, F.Dynys, O.Stephan, M.Walls, Ultramicroscopy, 2011, 11111, 169

54. D. C. Sinclair, T. B. Adams, F. D. Morrison, and A. R. West, Appl. Phys. Lett. 2002, 80, 2153.

55. P.R. Bueno and J. A. Varela, Materials Research, Vol. 9, No. 3, 293-300, 2006

56. E. R. Leitte, A. M. Nascimento, P. R. Bueno, E. Longo, J. A. Varela, J Mater. Sci.: Mater. Electron. 1999, 10, 321

57. A. Marzeca, M. Radeckab, W. Maziarzc, A. Kusiorb, Z. Pedzicha, J. Eur. Ceram. Soc. 2016, 36, 2981.

58. M. Radeckaa, P. Pasierba, K. Zakrzewskab, M. Rekas Solid State Ionics, 1999, 119, 43.

59 L.F. Lvovivh, Impedance Spectroscopy – Applications to Electrochemical and Dielectric Phenomena, 2012, Wiley, New Jersey, pp89-90

60 T.Q. Nguyen and C. Breitkopf, J. Electrochem. Soc., 165, E826 (2018)

61. C. Lei, A. A. Bokov, and Z.-G. Ye, J. Appl. Phys. 2007, 101, 084105.

62. J-P. Maria, X. Kang, R.D. Floyd, E.C. Dickey, H. Guo, J. Guo, A. Baker, S. Funihashi and C.A. Randall, J. Mater. Res., 2017, 32, 3205.

63. D. Wang, H. Guo, C.S. Morandi, C.A. Randall and S. Trolier-McKinstry 2018 *APL Materials* **6**, 016101

64. R. A. McKee, F. J. Walker, and M. F. Chisholm 1998 *Phys. Rev. Lett.* **81**, 3014

65. G. Niu, G. Saint-Girons, B. Vilquin, G. Delhaye, J.-L. Maurice, C. Botella, Y. Robach, and G. Hollinger 2009 *Appl. Phys. Lett*. **95**, 062902

66. J. H. Haoa and J. Gao 2005 *Appl. Phys. Lett*. **87**, 131908

67. G. Saint-Girons, R. Bachelet, Rahma Moalla, Benjamin Meunier, Lamis Louahadj, B. Canut, A. Carretero-Genevrier, J. Gazquez, P. Regreny, C. Botella, J. Penuelas, M.G. Silly, F. Sirotti, and G. Grenet 2016 *Chem. Mater*. **28** 5347

68. L. Mechin, G.J. Gerritsma, J. Garcia Lopez 1999 *Physica C* **324** 47

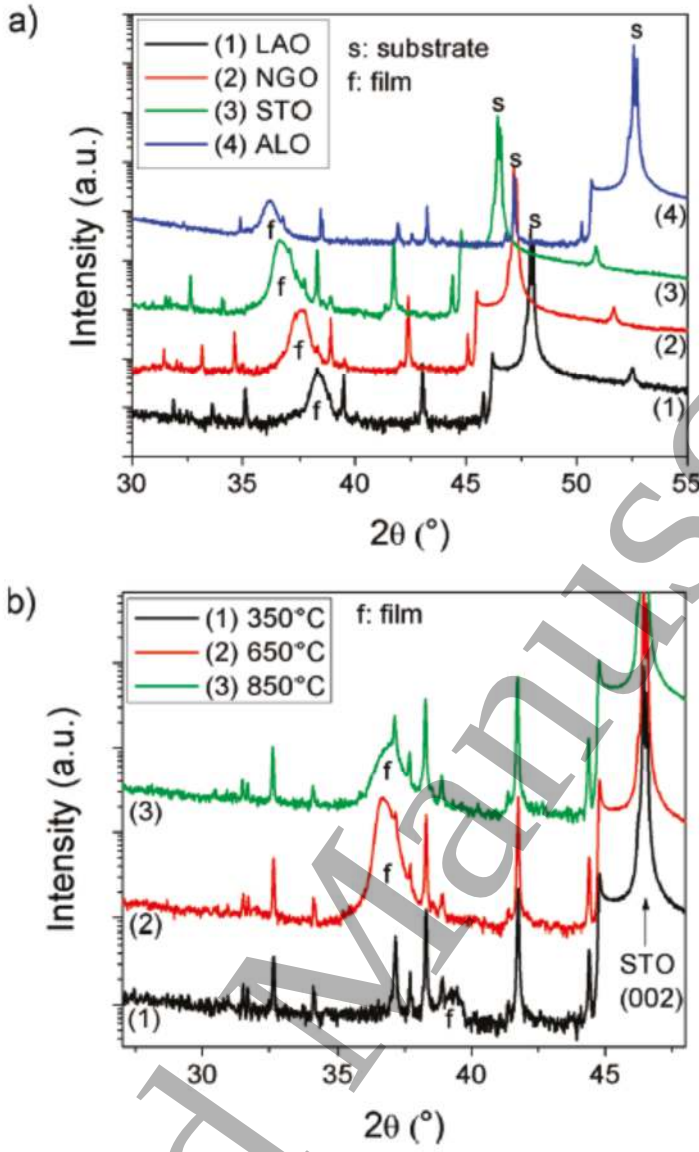

Figure 1: Powder X-ray diffraction patterns of $SnTiO_3$ films grown by Driscoll et al. showing (a) films deposited on a range of substrates and (b) films deposited on STO (001) at various temperatures. Reprinted with permission from Fix et al. Cryst. Growth Des. 2011, 11, 1422. [16] Copyright 2011 American Chemical Society.

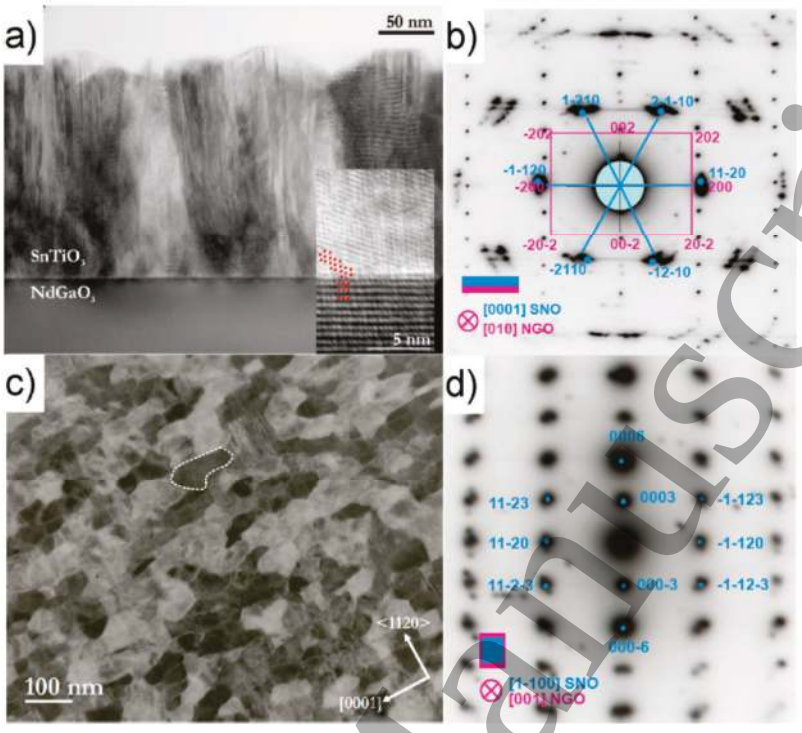

Figure 2: $SnTiO_3$ films grown by Driscoll et al. showing: (a) HRTEM image of film cross section, (b) diffraction pattern of with NGO [010] zone axis (hexagonal indexing), (c) TEM image (plan-view) of film and (d) diffraction pattern of with NGO [010] zone axis with hexagonal indexing (plan-view). Reprinted with permission from Fix et al. Cryst. Growth Des. 2011, 11, 1422. [16] Copyright 2011 American Chemical Society.

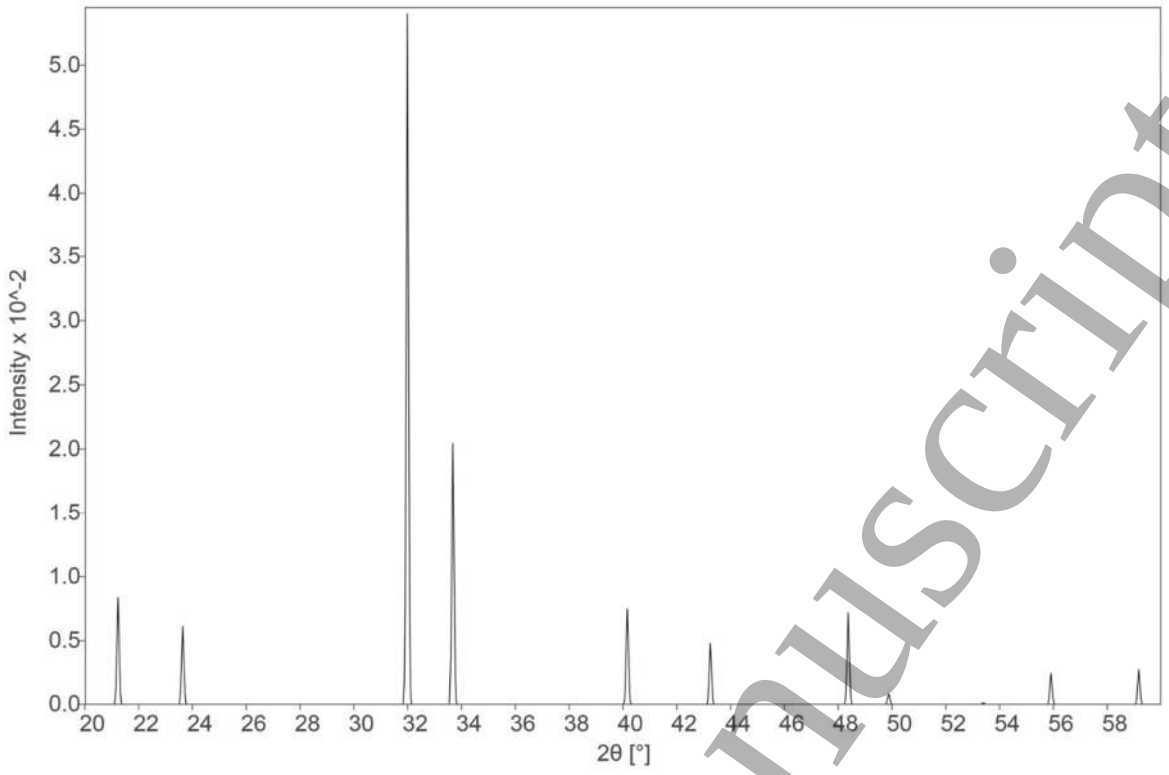

Figure 3: simulated PXRD pattern of perovskite structure (Cu $K\alpha_1$ radiation) using perovskite structural model (space group *P*4*mm*) and lattice parameters of possible minor perovskite phase from Ref. [16].

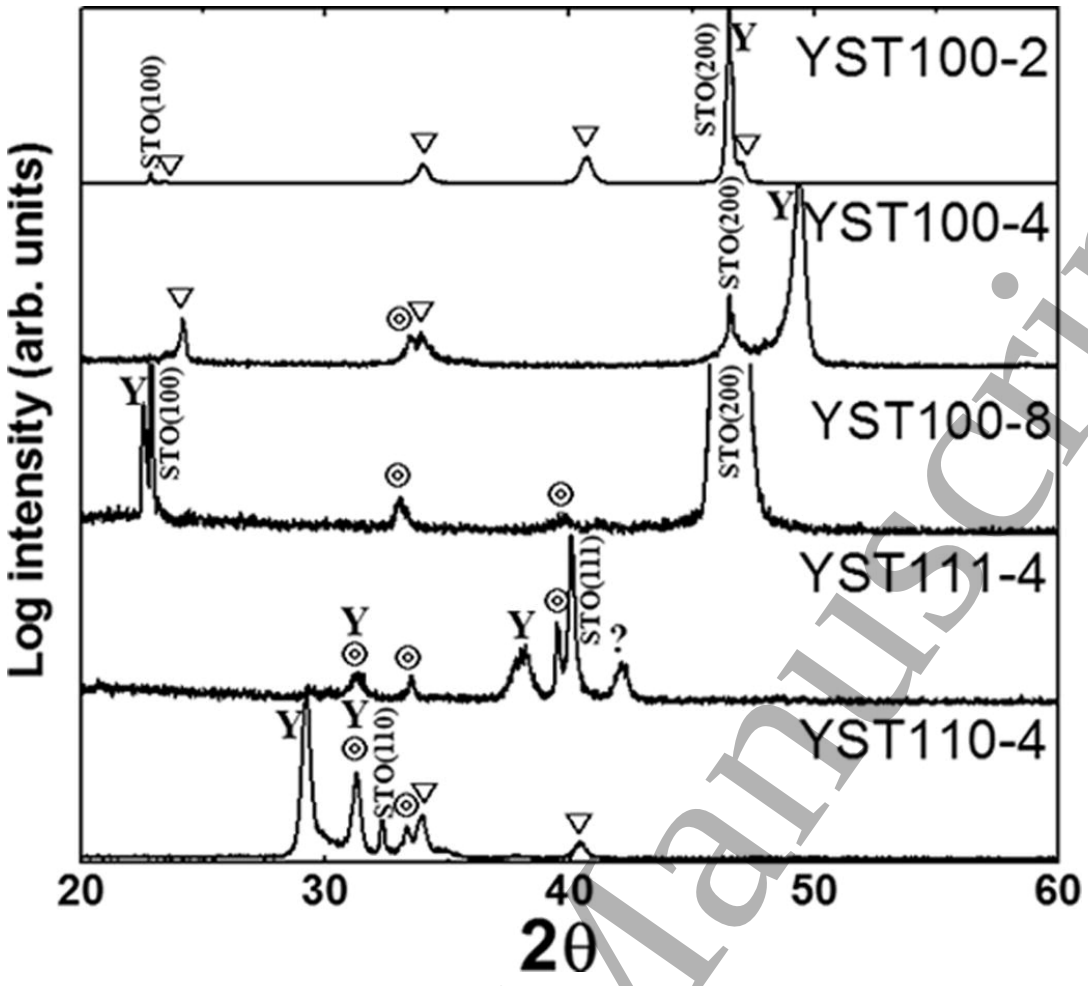

Figure 4: XRD of YMnO3/$SnTiO_{3+x}$ PLD films produced in Ref [19]. Films were deposited on 100, 111 or 110 orientated substrates with 4 or 8 layers - indicated in text on right of figure. Y = $YMnO_3$ phase, circle = perovskite, and triangle = ilmenite. Reprinted from "A new multiferroic heterostructure of $YMnO_3/SnTiO_{3+x}$", H Zhao *et al*., Scripta Materialia 65 (2011) 618, Copyright (2011), with permission from Elsevier and Acta Materialia Inc.

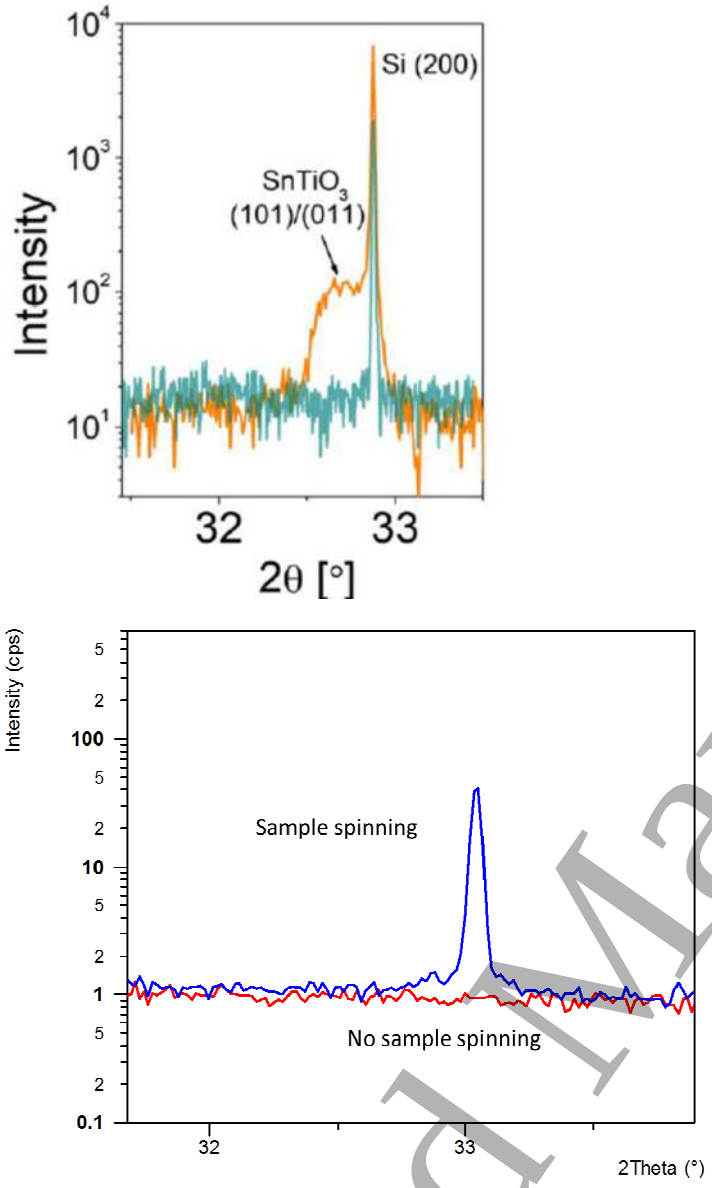

Figure 5: Powder X-ray diffraction patterns of: (a) Si(100) substrate (green) and deposited ALD film on substrate (orange), with the forbidden Si(200) and overlying peak, proposed to originate from perovskite SnTiO3, indicated (Reproduced from Ref [17], R. Agarwal, et al., Phys. Rev. B 2018, 97, 054109; (b) loss of forbidden Si(200) peak when sample sample is not spun.

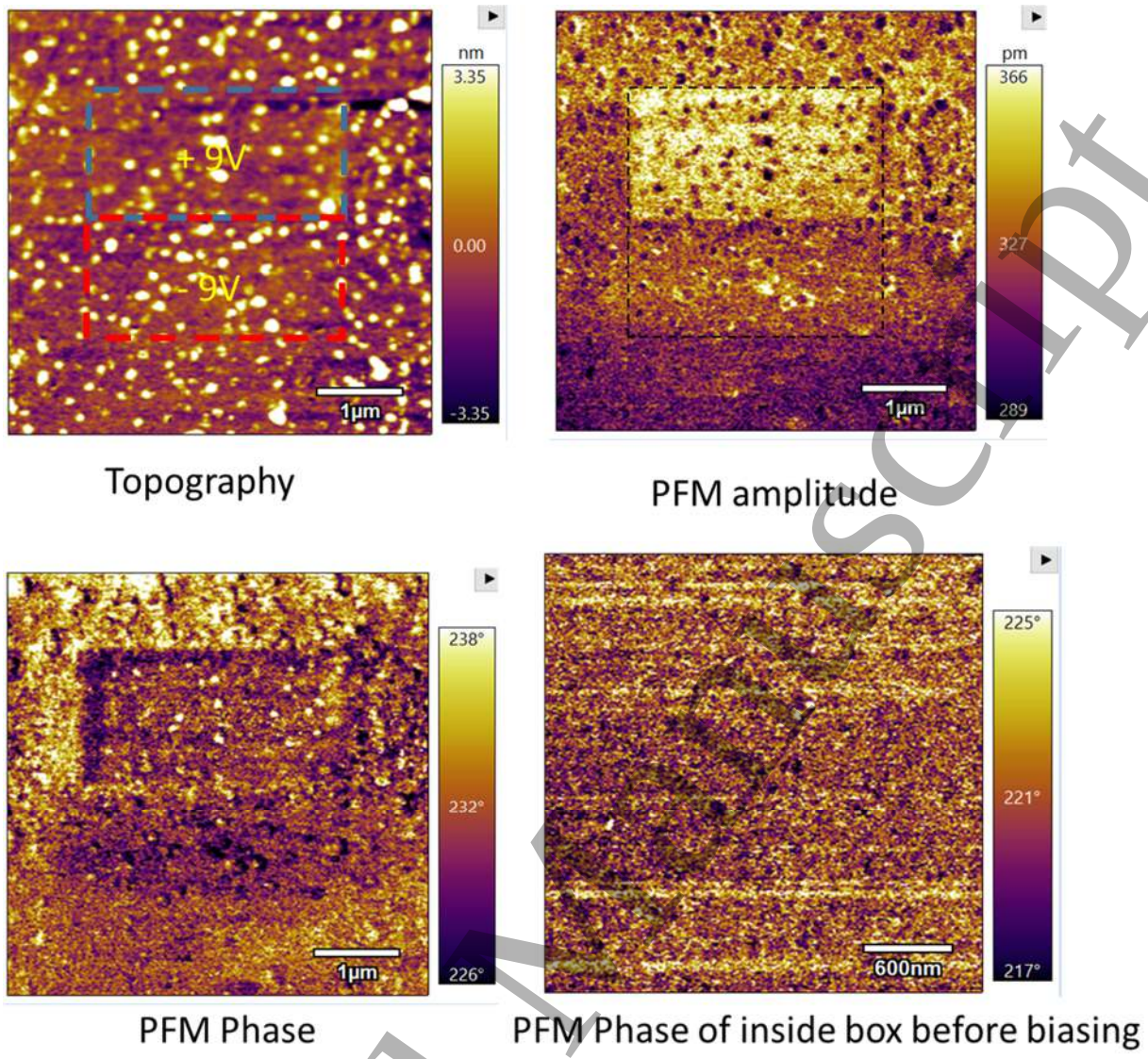

Figure 6: Piezoresponse force microscopy of ALD film. Contrast in phase and amplitude show contrast suggestive of bias writing.

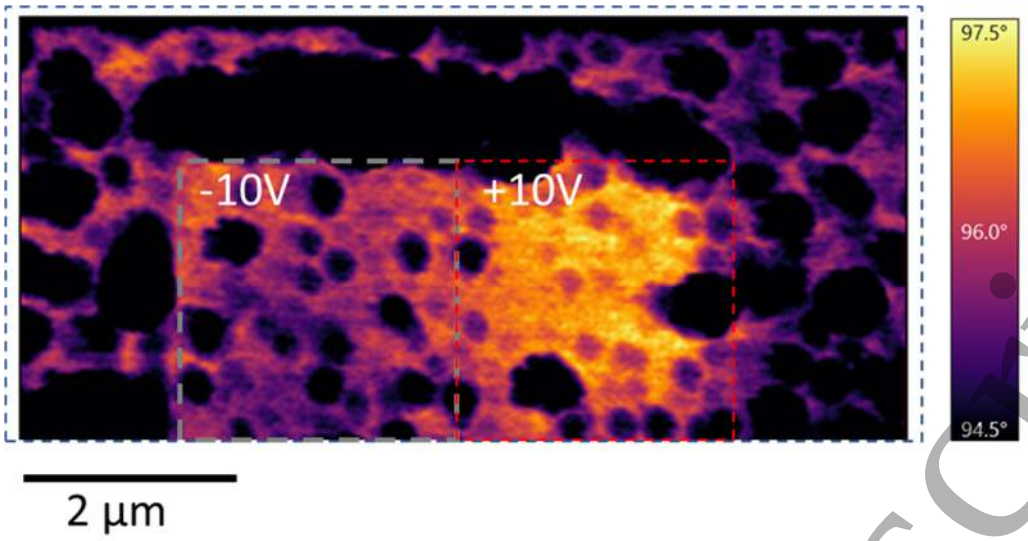

Figure 7: Electrical force microscopy of ALD film.

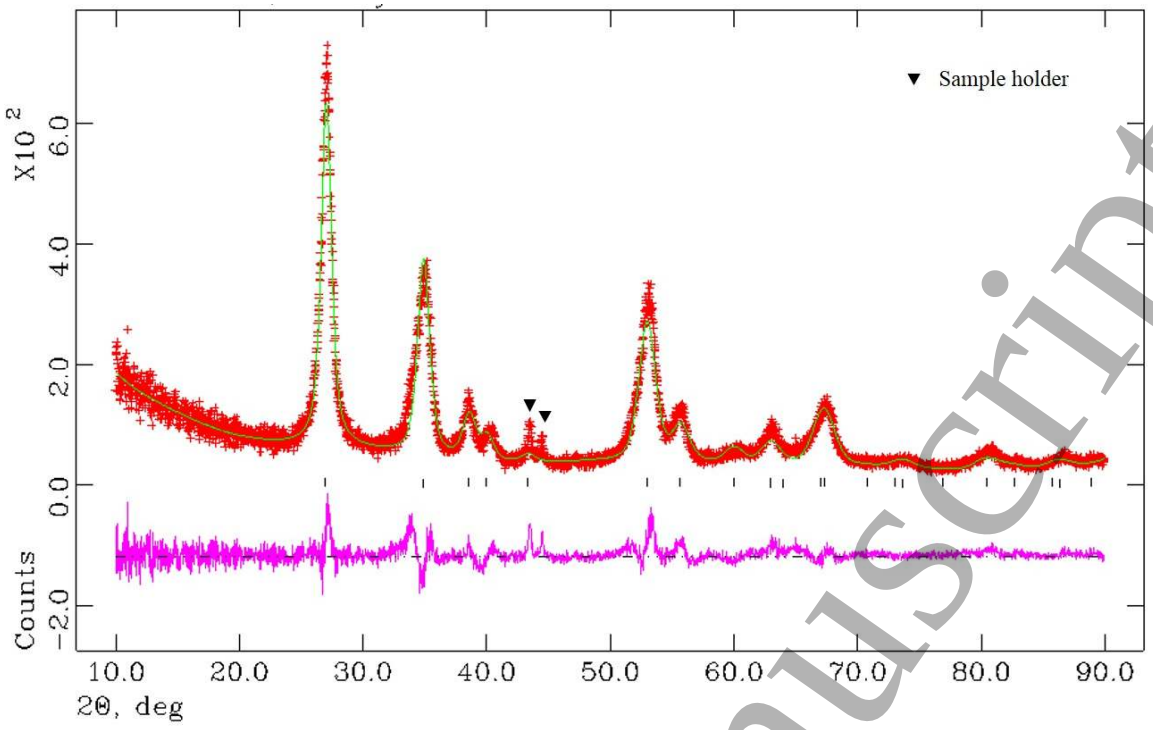

Figure 8: powder x-ray diffraction pattern of new sol-gel tin titanate. Bragg peaks are consistent with the rutile structure. Red crosses indicate observed data, vertical bars indicate reflection positions of rutile structure. The continuous line through the data represents the calculated structure from the Rietveld refinement; difference curve below this.

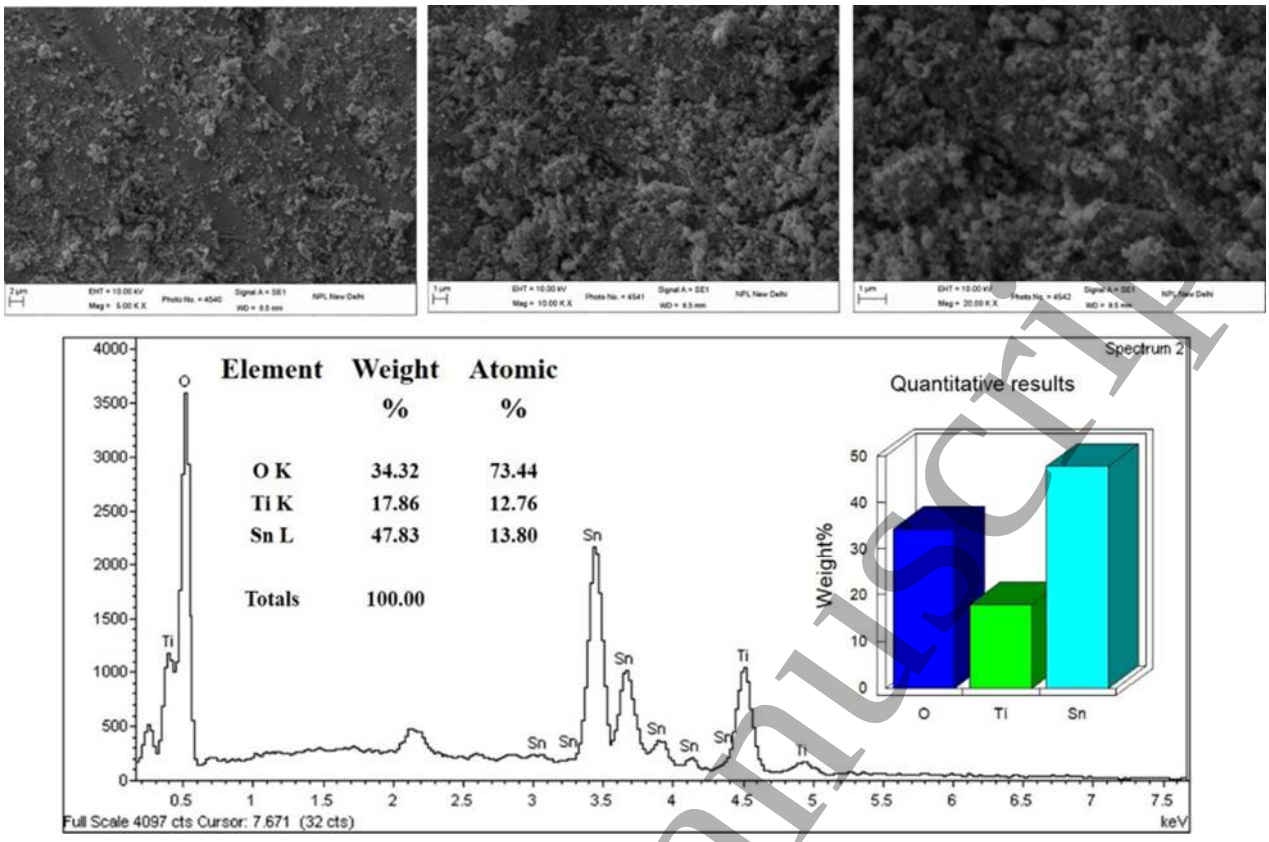

Fig. 9: illustrates the SEM/EDAX data, which demonstrate a 1.1:1 ratio of Sn/Ti in the new sol-gel samples, with 12.8% (atomic) Sn and 13.8% Ti and 73% oxygen.

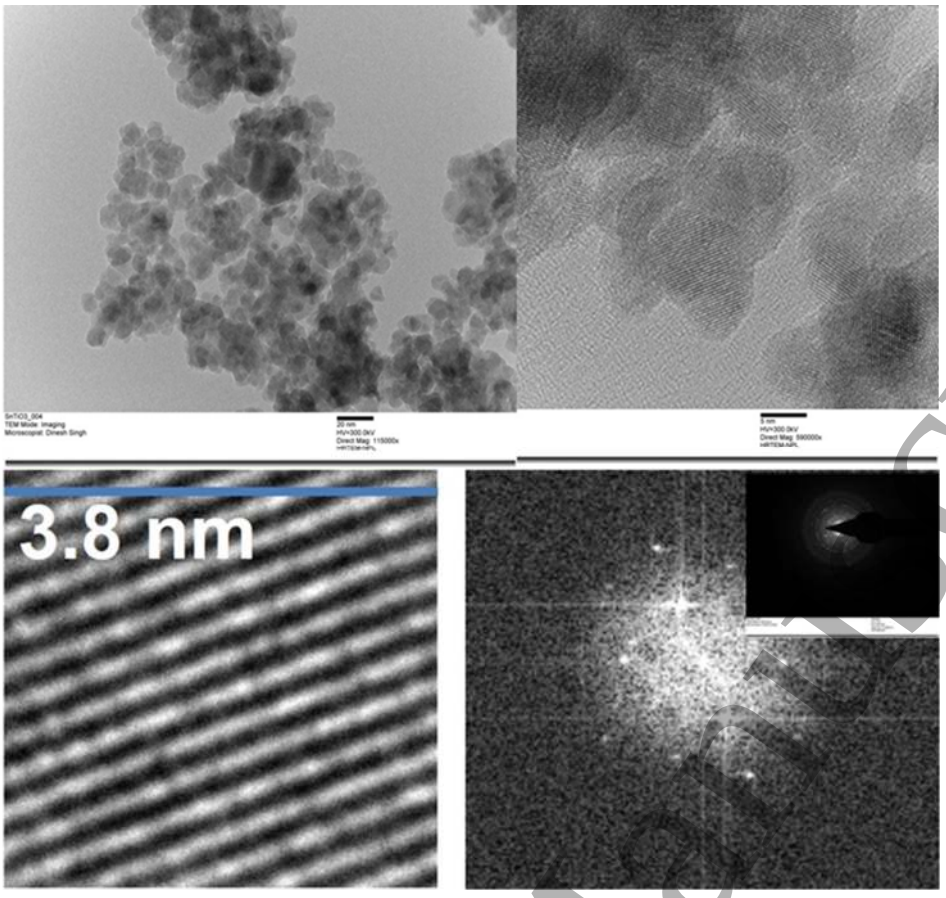

Fig. 10 depicts the high resolution TEM image of $SnTiO_3$ nanocrystals.

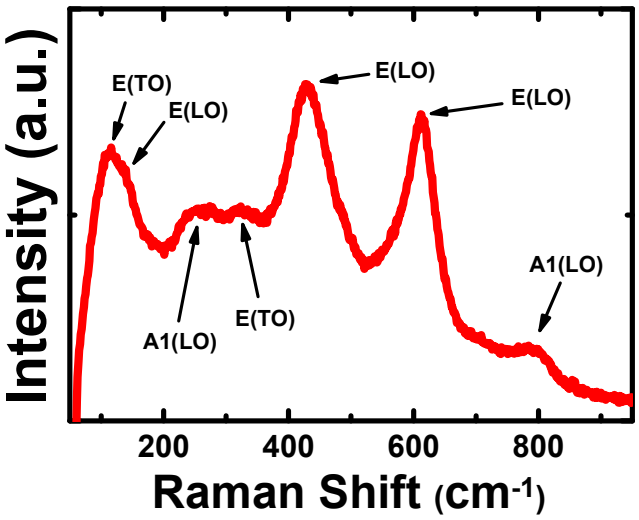

Fig. 11 Raman spectrum of tin titanate sample synthesised via sol gel route.

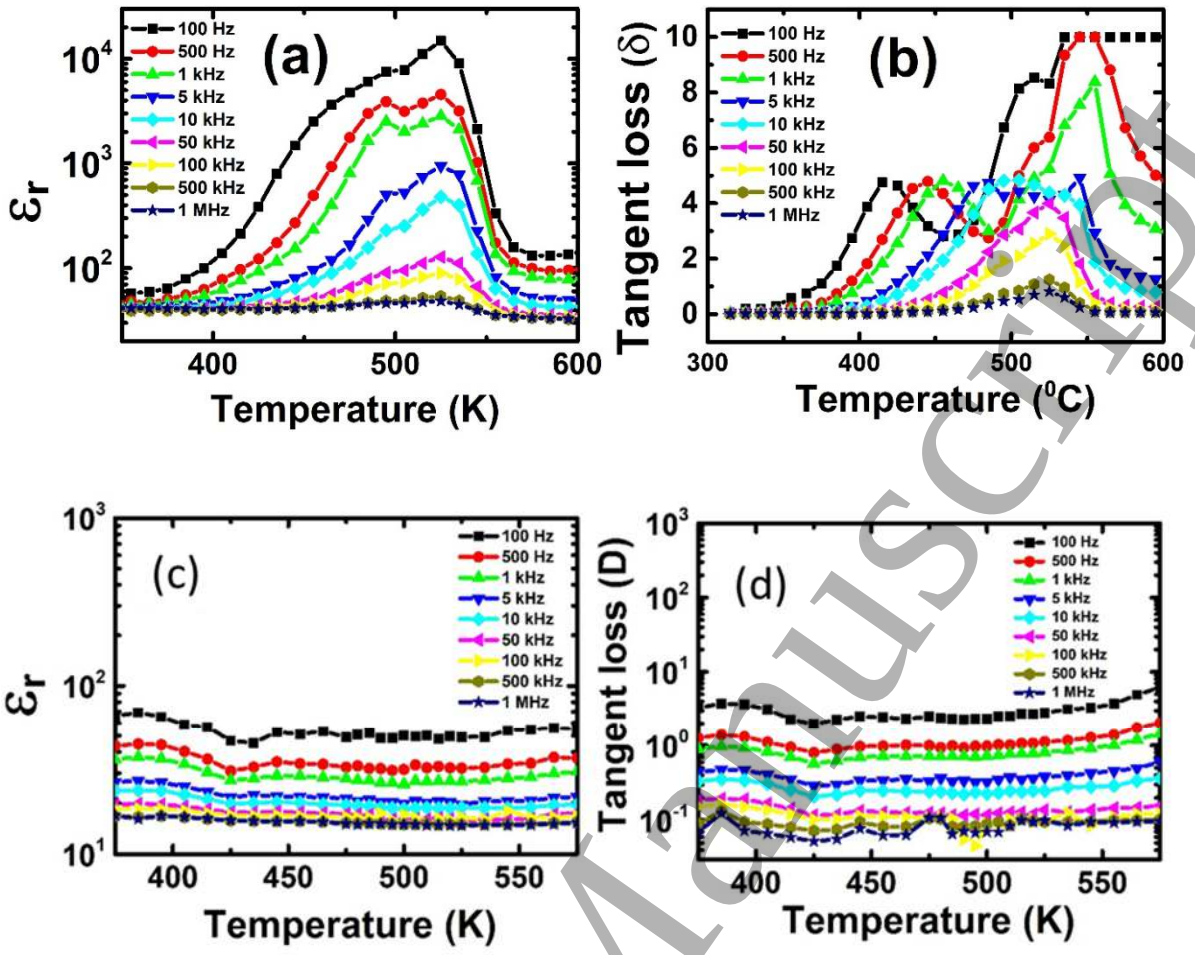

Figure 12: Relative permittivity, ε_r and normalised loss, tan δ, for tin titanate sol-gel pellets with Ag electrodes for: (a) and (b) initial heating and (c) and (d) subsequent cooling showing diminished peak.

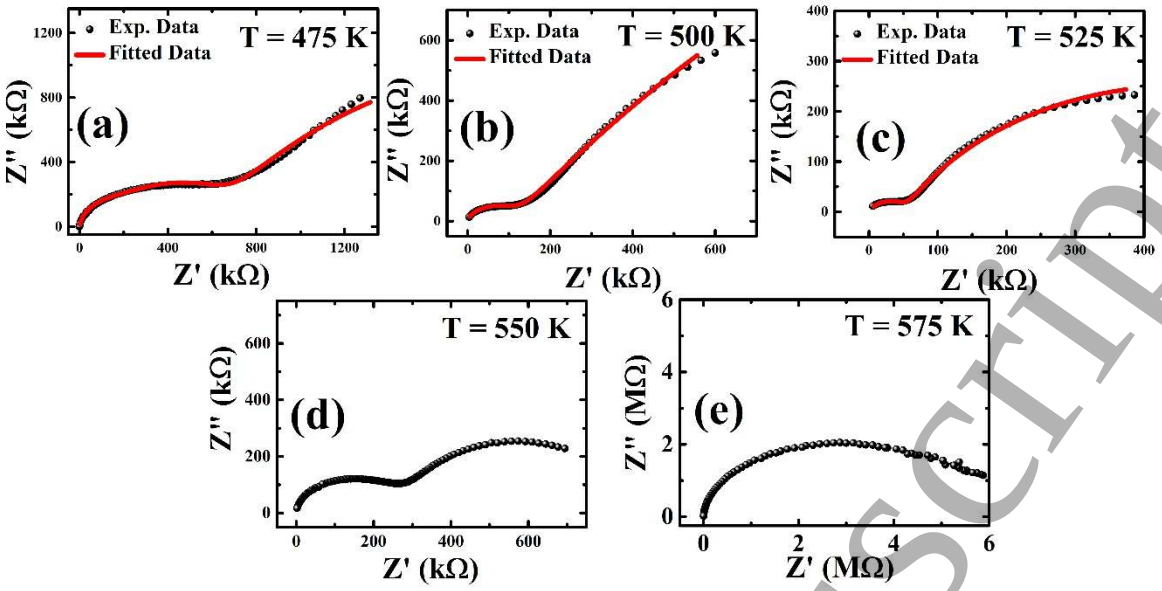

Figure 13: Impedance complex plane plots measured from tin titanate sol gel sample at different temperatures with equivalent electrical circuit model fitting.

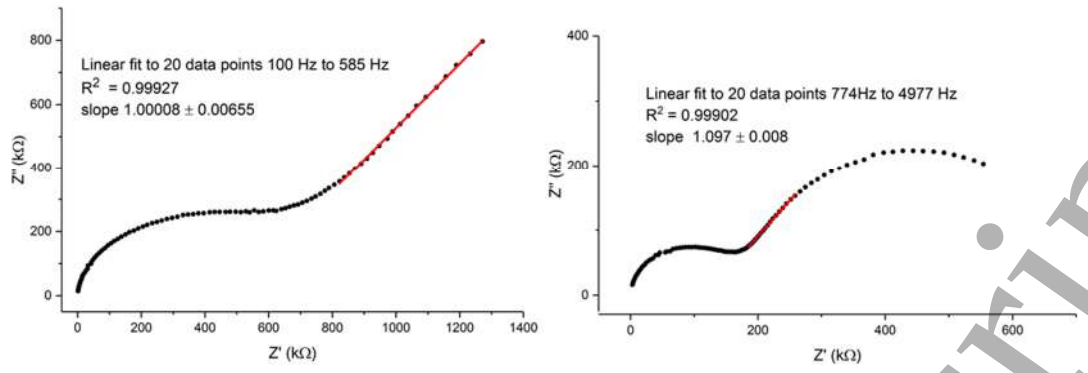

Figure 14: linear fit to low frequency data indicating Warburg element behaviour (gradient of fitted line ≈ 1) at 475 K and (right) apparent linearity present at higher temperatures (gradient of fitted line ≈ 1.1) at 540 K.

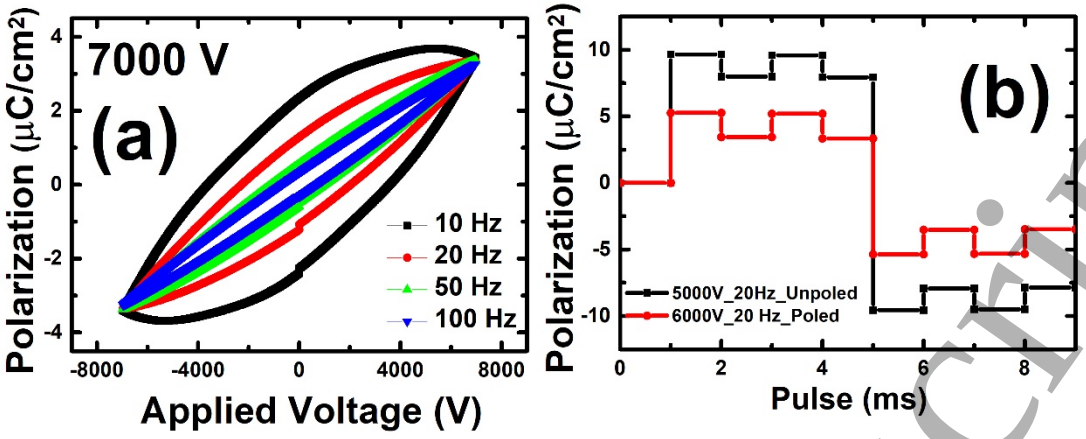

Figure 15: (a) Polarisation vs. applied voltage plot of the tin titanate sol gel sample, (b) PUND data of the bulk sample in unpoled and poled situation.